ChemComm

Discovery of an Olivine-type Lithium Manganese Thiophosphate, LiMnPS4, via Building Block Approach

Journal:	*ChemComm*
Manuscript ID	CC-COM-09-2021-005168.R1
Article Type:	Communication

COMMUNICATION

Discovery of an Olivine-type Lithium Manganese Thiophosphate, $LiMnPS_4$, via Building Block Approach†

*Srikanth Balijapelly,[a] Kartik Ghosh,[b] Aleksandr V. Chernatynskiy,[c] Amitava Choudhury[a,] **

Received 00th January 20xx,
Accepted 00th January 20xx

DOI: 10.1039/x0xx00000x

An olivine-type orthothiophospate $LiMnPS_4$ has been synthesized for the first time through building block approach by reacting preformed ternary lithium thiophospate with $MnCl_2$. Diffuse reflectance measurements show an optical band gap of 2.36 eV which is further confirmed by DFT calculations. Irreversible weak ferromagnetic ordering and metamagnetism are verified through priliminary magnetic measurements.

Transition metal oxy-phosphates are ubiquitous as they are found in mineral kingdom and easily made in the laboratory.[1, 2] A large number of oxy-phosphates especially ortho-phosphates of transition metals have been synthesized in the last couple of decades as these materials became potential candidates for electrodes and solid-electrolytes in Li- and Na-ion batteries.[3-5] On the other hand, as of now there is no report of any chalcophosphate mineral;[6] as they can only be accessed through laboratory synthesis.[7-21] Synthetic chalco-phosphates can form a myriad of chalcophosphate anions, $[P_xQ_y]^{z-}$, that includes $[PQ_4]^{3-}$,[8,9, 11, 13, 14] $[P_2Q_6]^{4-}$,[7, 12, 17, 18] $[P_2Q_7]^{4-}$,[10] $[P_2Q_9]^{4-}$,[16] $[P_5Q_{12}]^{5-}$,[19] $[P_6Q_{12}]^{4-}$,[19, 20] and many others. In most of these chalco-phosphate building blocks P is formally in +5 oxidation state except when P – P bond is present, where it is +4 as in $[P_2Q_6]^{4-}$. These $[P_xQ_y]^{z-}$ units can be stabilized with alkali ions or with metals; transition or main-group metals. Several groups, namely Kanatzidis,[10, 13, 18-20] Dorhout,[12, 16] Schleid,[14] Bensch,[15] Lotsch[17] and others,[7, 8, 9, 11] have extensively investigated synthesis of new ternary and quaternary chalco-phosphates either from elements or using binaries often in presence of polychalcogenide or poly-chalcophosphate flux. These reactions involving rare-earth metals mainly led to ortho-chalcophosphates[12, 13, 14, 15] or hexachalcohypodiphosphates[12, 17] often incorporating alkali ions. However, with 1st row transition series it has rarely formed ortho-chalcophosphates because of the high prevalence of $[P_2Q_6]^{4-}$ unit. To our knowledge there are only a few examples of ortho-thiophosphate structure in 1st row transition metal, $KNiPS_4$,[8] $NaTi_2(PS_4)_3$,[9] $Na_3Cr_2(PS_4)_3$,[11] and Cu_3PS_4.[21] There is a renewed interest in the synthesis and crystal growth of chalco-phosphates especially in layered two-dimensional (2D) materials with van der Waals gap ($M_2P_2Q_6$, M = 1st row transition metals) and non-vdW 2D materials with intercalated alkali ions ($A_2MP_2S_6$, A = Li, K) for their magnetism and other exotic phenomena in low dimensions.[22-26] 2D $M_2P_2Q_6$ compositions are well-known cathode material[27] and there is a growing interest in chalco-phosphates as electrode materials.[28-30] In this connection we asked ourselves why it is difficult to synthesize ortho-thiophosphates of transition metals analogous to well-known structure types in ortho-(oxy)phosphates for example, olivine[3] and NASICON;[5] phases that have defined new direction in electrode materials.[4] Strong covalent bonding of chalco-phosphate moiety with transition metals can lead to semiconducting solid with intermediate range band gap useful for photovoltaics and presence of unfilled 3*d* electrons can give rise to magnetic and redox (batteries) properties, while a combination of both can have applications in spintronics and magnetoelectrics.[22-24] Hence, if the rich structural diversity of ortho-oxy phosphates is accessed in transition metal chalco-phosphates, a plethora of new properties can be expected.

Therefore, we have directed our efforts to synthesize ortho-thiophosphate of transition metals. We have employed an innovative building block approach in which lithium thiophosphate Li_3PS_4 consisting a preformed PS_4^{3-} tetrahedral building unit is reacted with $MnCl_2$ in so-called solid state metathesis reaction to create first ever olivine-type ortho-thiophosphate with transition metal, $LiMnPS_4$.

In this communication, we report the synthesis, crystal structure, optical, preliminary magnetic properties along with theoretical calculations within DFT framework to elucidate the electronic band structure.

$LiMnPS_4$ has been synthesized from solid-state metathesis route using γ-Li_3PS_4 and $MnCl_2$ in sealed evacuated quartz tube at 500 °C (for details, see ESI).

$$\gamma\text{-}Li_3PS_4 + MnCl_2 \rightarrow LiMnPS_4 + 2LiCl$$

[a]*Department of Chemistry, Missouri University of Science and Technology, Rolla, MO 65409, USA. E-mail: choudhurya@mst.edu*
[b]*Department of Physics, Astronomy and Materials Sci, Missouri State University, 901 S. National Ave., Springfield, MO 65897, USA*
[c]*Department of Physics, Missouri University of Science and Technology, Rolla, MO 65409, USA*

† *Electronic supplementary information (ESI) available: Details of the synthesis, crystal structure determination, calculations, and PXRDs.* See DOI: xxx

Pale yellow color crystals (Figure S1, ESI) were obtained after breaking the ampoule inside an argon-filled glove box. Crystal structure was determined from single-crystal X-ray diffraction. Crystal data and final refinement parameters are summarized in Table 1 and other crystallographic details are given in ESI (Tables S1 - S3). The laboratory powder X-ray diffraction (PXRD) pattern confirmed the phase purity of the bulk sample (Figure S2, ESI). The PXRD of γ–Li_3PS_4 and the air exposed (>24 hours) sample of $LiMnPS_4$ are provided in ESI (Figures S3 and S4, ESI). The PXRD of $LiMnPS_4$ after air exposure did not show any change indicating good air stability. EDS elemental analysis (Figure S5, ESI) performed on as-synthesized crystals is in good agreement with the crystallographic composition ($Mn_{1.04}P_{1.02}S_4$).

Table 1. Crystal data and refinement parameters for $LiMnPS_4$.

Empirical formula	$LiMnPS_4$
Temperature	300(2) K
Crystal system	Orthorhombic
Space group	*Pnma*
Unit cell dimensions	a = 12.540(3) Å
	b = 7.654(2) Å
	c = 5.834(2) Å
Volume	560.0(2) Å^3
Z	4
Goodness-of-fit on F^2	1.112
Final *R* indices [I>2σ(I)]	R_1 = 0.0330
R indices (all data)	wR_2 = 0.0852

$LiMnPS_4$ crystallizes in olivine structure type in *Pnma* space group. The asymmetric unit of $LiMnPS_4$ consists of one Mn (4*b*, Wyckoff site), one P (4*c*), one Li (4*c*) and three S (S1 in 8*a*, S2 and S3 in 4*c*) sites yielding a composition of $Li_{0.5}Mn_{0.5}P_{0.5}S_2$ (Figure 1a). If an empirical formula of $LiMnPS_4$ is used, then four such units (Z = 4) will be present in the unit cell. The structure of $LiMnPS_4$ can be described as hcp array of S atoms in which half of the octahedral sites in alternate layers are filled with Mn and Li atoms, respectively, while one-eighth of the tetrahedral holes are filled with P atoms. Such filling up of holes by Mn and P creates a situation where edge-shared MnS_6 octahedra form infinite chains parallel to the *b*-axis, which are further stitched together by PS_4 tetrahedral units forming layers perpendicular to *a*-axis. The interlayer space is filled by Li ions (Figure 1b).

The structure of $LiMnPS_4$ belongs to olivine-Mg_2SiO_4 structure type,[31] where Li and Mn replaces two crystallographically distinct Mg ions in 4*a* and 4*c* sites, respectively, and SiO_4 unit is replaced by PS_4 unit. However, there is a slight difference in the atomic positions when compared with the ortho-(oxy)phosphate analogue, olivine-$LiMnPO_4$ or in general, olivine-Li*M*PO_4 (*M* = Mn, Fe, Co, and Ni), all of which are well-known cathode materials for Li-ion batteries.[3, 4] In the thiophosphate analogue, the position of transition metal and lithium ion are interchanged when compared to $LiMnPO_4$ i.e. in oxy-phosphate 4*c* Wyckoff site is occupied by Mn ion whereas the same site is occupied by Li ion in the thiophosphate. Such switching of Li and Mn positions makes $LiMnPS_4$ a layered material meaning covalent connectivity between PS_4 and MnS_6 extends only in 2-dimensions and such layers are held together *via* predominantly ionic forces by intervening Li-ions. On the other hand, $LiMnPO_4$ has three-dimensional structure with one-dimensional channels filled with Li-ions. Hence, $LiMnPS_4$ can be considered as the first example of chalco-phosphate olivine analogue of the well investigated $LiMnPO_4$.

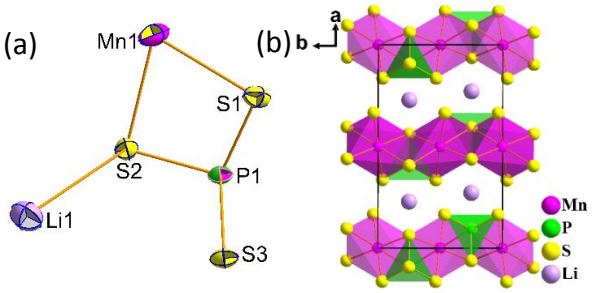

Figure 1. (a) Asymmetric unit of $LiMnPS_4$; (b) Layers formed by parallel chains of MnS_6 edge sharing octahedra connected by PS_4 tetrahedra separated by interlayer octahedrally coordinated Li ions.

Considering our implemented metathesis synthesis method, it is worth comparing the structure of starting material, γ-Li_3PS_4 or its polymorph, β-Li_3PS_4 with $LiMnPS_4$. γ-Li_3PS_4 is the room temperature polymorph, which on heating undergoes phase transition to superionic phase β-Li_3PS_4.[32] It is to be noted here that β-Li_3PS_4 is very close to olivine, out of the three Li-sites one of the Li occupies an octahedral site (4*b*) same as Li in $LiMnPO_4$. However, it has two additional Li-sites which are tetrahedral and not filled in olivine. On close inspection it is found that $LiMnPS_4$ can be topotactically generated from the high temperature polymorph β-Li_3PS_4. The Figure 2 shows the structural comparison of β-Li_3PS_4, $LiMnPS_4$, and $LiMnPO_4$. During the solid-state metathetic reaction with $MnCl_2$, the starting reaction precursor, γ-Li_3PS_4, transforms to β-Li_3PS_4 above 200 °C and octahedral Li(Li2) is substituted by Mn followed by a change in coordination of Li1 from tetrahedral to octahedral coordination leading to the formation of $LiMnPS_4$ with the elimination of tetrahedral Li(Li3) site as one Mn^{2+} will compensate charges for two Li^+ ions. This is the innovativeness of our building block approach which enabled retention of the building block, ortho-thiophosphate unit, and led to the discovery of olivine phase, $LiMnPS_4$.

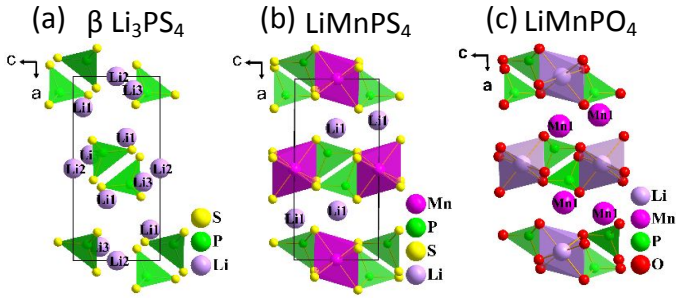

Figure 2. Comparing the crystal structures of (a) β – Li_3PS_4; (b) $LiMnPS_4$;(c) $LiMnPO_4$.

The traditional solid-state synthesis using elements in chalco-phosphate flux is perceived as the most viable way to synthesize transition metal thiophosphates.[10, 26] Metathesis reactions have also been employed in some cases, for example, reaction between $Li_4P_2S_6$ and Ni^{2+} salt in aqueous medium yielded poorly crystalline $Ni_2P_2S_6$;[33] a mixed metal seleno-phosphate,

$M^{+1}M^{+3}P_2Se_6$ has been synthesized by reacting $M^{+1}Cl$ and $M^{+3}Cl_3$ with $Mg_2P_2S_6$.[34, 35] Metathesis reactions offer advantage over typical solid state reactions using elements or flux in terms of lower reaction temperatures, better control over the product formation and often allows rational design when the reaction is topotactic.[36] The formation enthalpy of the salt byproduct in metathesis reactions drive the reaction in forward direction. This is the first report of metathesis reaction with a preformed PS_4^{3-} building unit with transition metal chloride salt. This novel synthetic route can give access to new materials which otherwise may not have been discovered through traditional solid-state elemental or flux-based reactions.

From the charge neutral formula, $LiMnPS_4$, it can be expected to have semiconductor-like band gap. Accordingly, the optical band gap is found to be 2.36 eV from the diffuse reflectance spectra as shown in Fig 3a (details in ESI). The optical band gap of γ-Li_3PS_4 is found to be 3.8 eV (Figure S6, ESI), therefore, the topotactic insertion of Mn for Li ion in Li_3PS_4 reduces the band gap by ~1.5 eV. Weak spin-forbidden *d-d* transitions due to high spin Mn(II) can be seen before the steep jump due to band gap (Figure 3b). To understand the origin of this band gap narrowing, we performed spin polarized band structure calculations on experimentally determined structure using density functional theory (DFT) as implemented in VASP. Further details of DFT calculations are given in ESI. The calculated band gap of 2.3 eV using HSE06 hybrid functional (Figure 3c) is in very good agreement with the experimentally obtained band gap of 2.36 eV. The projected density of states for $LiMnPS_4$ calculated using HSE06 hybrid functional is shown in Figure 3c (Figure S7, ESI). The top of the valence band has the contribution mainly from S *p* states and Mn *d* states, whereas the bottom of the conduction band has major contribution from S *p* and P *s* states. Contribution of Li ions is almost negligible near the Fermi level. Figure 3d shows the electronic band

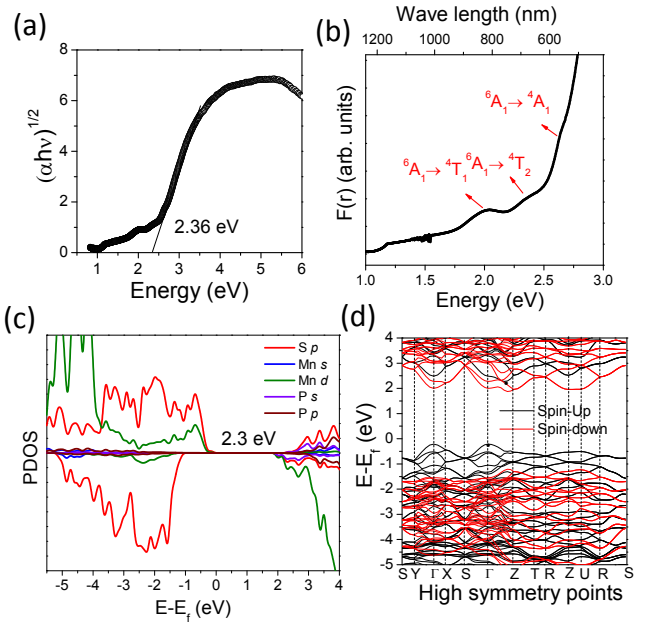

structure along the high symmetry points in the Brillouin zone of orthorhombic lattice. The valence band maximum occurs at Γ point and the conduction band minimum occurs close to Z point of the Brillouin zone confirming that $LiMnPS_4$ is an indirect band gap material. The indirect nature of the band gap agrees well with the experimental DRS measurements.

Figure 3. (a) Diffuse reflectance plot of $LiMnPS_4$; (b) Spin forbidden weak *d* – *d* transitions; (c) Partial density of states of $LiMnPS_4$; (d) Band structure of $LiMnPS_4$.

Magnetic Properties

Temperature dependence of magnetic susceptibility and inverse susceptibility of $LiMnPS_4$ measured at an applied field of 1T from 3.2K to room temperature are given in Figure 4a. The molar magnetic susceptibility (χ_M) increases asymptotically and reaches a maximum at 28 K and after that there is a sharp fall of χ_M indicating onset of antiferromagnetic ordering below 28K. The temperature dependence of the inverse magnetic susceptibility, χ_M^{-1}(T), shows linear behavior between 150-300K which can be fitted with Curie-Weiss law yielding a Curie constant of 4.045 emu.K.mol^{-1} and a Weiss constant (θ_p) of –52.29 K, respectively. Large negative, θ_p, value indicates strong antiferromagnetic interactions between adjacent Mn(II) ions. The experimental magnetic moment per Mn derived from Curie constant is 5.69 μ_B, which is close to the spin only magnetic moment 5.92 μ_B for high spin Mn^{2+} with five unpaired electrons. To understand the nature of antiferromagnetic transition, dc magnetization measurements were performed under field cooled (FC) and zero field cooled (ZFC) conditions under low applied field of 0.1T (Figure 4b). The FC and ZFC magnetic susceptibilities show an obvious divergence below 24 K, which could be due to irreversible weak ferromagnetic transition resulting from spin canting. The presence of weak ferromagnetic transition at lower applied fields and disappearance at higher applied field indicates field-induced metamagnetic transition. Variable field isothermal magnetization measured at 300K shows sluggish increase in the

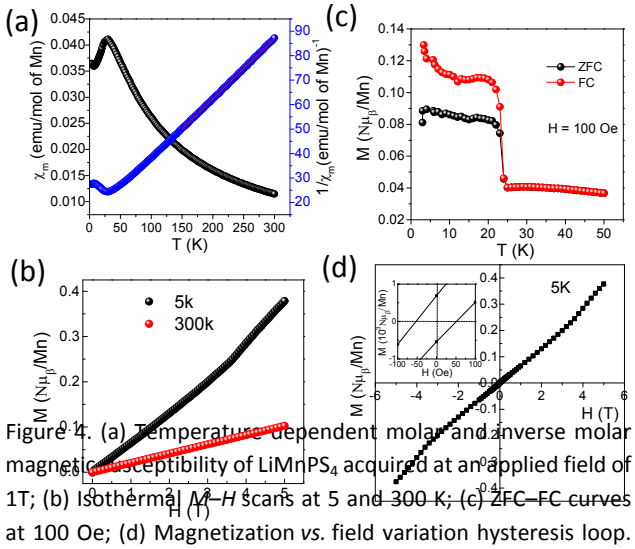

Figure 4. (a) Temperature dependent molar and inverse molar magnetic susceptibility of $LiMnPS_4$ acquired at an applied field of 1T; (b) Isothermal *M*–*H* scans at 5 and 300 K; (c) ZFC–FC curves at 100 Oe; (d) Magnetization *vs.* field variation hysteresis loop. Inset shows an enlargement view of the remanent magnetization around the zero-field strength.

magnetization to 0.11Nβ whereas at 3K magnetization gradually increases to 0.25 Nβ, after that a steep rise from 0.25 to 0.38 Nβ between 3.75 and 5T, respectively (Figure 4c), indicating a field-induced metamagnetic transition from antiferromagnetic to ferromagnetic state. A small but detectable hysteresis loop (inset, Figure 4d) was also observed.

Metamagnetism has been observed in many compounds containing Mn(II) chains with various bridging networks.[37-39] Because of the presence of the inversion centers between the adjacent Mn(II) ions, rules out the occurrence of antisymmetric interactions, however, at much lower temperatures, slight distortion in the crystal structure could cause spins to be tilted away from the antiparallel arrangement causing weak ferromagnetic ordering.

In summary, we reported a new quaternary sulfide, $LiMnPS_4$, with olivine structure synthesized for the first time through solid-state metathesis route using preformed Li_3PS_4 and $MnCl_2$. Parallel chains of edge shared MnS_6 connected by PS_4 tetrahedral units form 2D layers, where the interlayer space is occupied by Li ions. $LiMnPS_4$ possess an indirect band gap of 2.36 eV which is further confirmed by HSE06 calculations. Preliminary magnetic measurements confirm the field induced metamagnetic transition resulting from spin canting. This work emphasizes that chalco-analogues of oxy-(ortho)phosphate structures can be accessed through solid-state metathesis route by employing building block approach.

Author Contributions

AC conceived the problem and supervised the work. SB carried out experimental work and performed theoretical calculations. AVC supervised theoretical calculations. KG helped with magnetic measurements. SB and AC wrote the manuscript, and all the authors approved the manuscript and provided their feedback.

Conflicts of interest

There are no conflicts to declare.

Acknowledgements

The authors thank NSF (grant No. DMR- 1809128) for funding.

Notes and references

1 Nriagu, J.O. Phosphate Minerals: Their Properties and General Modes of Occurrence. In: *Phosphate Minerals* (J.O. Nriagu and P.B. Moore, Eds.), Springer-Verlag, Heidelberg, 1984; pp. 1–136.
2 R. Murugavel, A. Choudhury, M. G. Walawalkar, R. Pothiraja and C. N. R. Rao, *Chem. Rev.*, 2008, **108**, 3549–3655.
3 A. K. Padhi, K. S. Nanjundaswamy and J. B. Goodenough, *J. Electrochem. Soc.*, 1997, **144**, 1188.
4 C. Masquelier and L. Croguennec, *Chem. Rev.*, 2013, **113**, 6552–6591.
5 K. Arbi, W. Bucheli, R. Jiménez and J. Sanz, *J. Eur. Ceram. Soc.*, 2015, **35**, 1477–1484.
6 Y. Moëlo, E. Makovicky, N. N. Mozgova, J. L. Jambor, N. Cook, A. Pring, W. Paar, E. H. Nickel, S. Graeser, S. Karup-Møller, T. Balic-Žunic, W. G. Mumme, F. Vurro, D. Topa, L. Bindi, K. Bente and M. Shimizu, *Eur. J. Mineral.*, 2008, **20**, 7–46.
7 G. Ouvrard, R. Brec and J. Rouxel, *Mater. Res. Bull.*, 1985, **20**, 1181–1189.
8 S. H. Elder, A. Van der Lee, R. Brec and E. Canadell, *J. Solid State Chem.*, 1995, **116**, 107–112.
9 X. Cieren, J. Angenault, J. C. Couturier, S. Jaulmes, M. Quarton and F. Robert, *J. Solid State Chem.*, 1996, **121**, 230–235.
10 Jason A. Hanko, Julien Sayettat, Stéphane Jobic, and Raymond Brec and Mercouri G. Kanatzidis, *Chem. Mater.*, 1998, **10**, 3040–3049.
11 S. Coste, E. Kopnin, M. Evain, S. Jobic, C. Payen and R. Brec, *J. Solid State Chem.*, 2001, **162**, 195–203.
12 C. R. Evenson and P. K. Dorhout, *Inorg. Chem.*, 2001, **40**, 2884–2891.
13 J. A. Aitken and M. G. Kanatzidis, *J. Am. Chem. Soc.*, 2004, **126**, 11780–11781.
14 P. L. Lange and T. Schleid, *Eur. J. Inorg. Chem.*, 2021, (32) 3247-3254
15 Y. Klawitter, W. Bensch and C. Wickleder, *Chem. Mater.*, 2005, **18**, 187–197.
16 J. M. Knaust and P. K. Dorhout, *J. Chem. Crystallogr. 2005 363*, 2006, **36**, 217–223.
17 L. M. Schoop, R. Eger, R. K. Kremer, A. Kuhn, J. Nuss and B. V. Lotsch, *Inorg. Chem.*, 2017, **56**, 1121–1131.
18 A. S. Haynes, C. C. Stoumpos, H. Chen, D. Chica and M. G. Kanatzidis, *J. Am. Chem. Soc.*, 2017, **139**, 10814–10821.
19 I. Chung, J. I. Jang, M. A. Gave, D. P. Weliky and M. G. Kanatzidis, *Chem. Commun.*, 2007, 4998–5000.
20 I. Chung, A. L. Karst, D. P. Weliky and M. G. Kanatzidis, *Inorg. Chem.*, 2006, **45**, 2785–2787.
21 J. Garin, and E. Parthe, *Acta Cryst.*, 1972, **B28**, 3672-3674.
22 M. A. Susner, M. Chyasnavichyus and M. A. Mcguire, *Adv. Mater.*, 2017, **29**, 1602852.
23 C. C. Mayorga-Martinez, Z. Sofer, D. Sedmidubský, Š. Huber, A. Y. S. Eng and M. Pumera, *ACS Appl. Mater. Interfaces*, 2017, **9**, 12563–12573.
24 Y. Zhang, T. Fan, S. Yang, F. Wang, S. Yang, S. Wang, J. Su, M. Zhao, X. Hu, H. Zhang and T. Zhai, *Small Methods*, 2021, **5**, 2001068.
25 T. J. Diethrich, P. Y. Zavalij, S. Gnewuch and E. E. Rodriguez, *Inorg. Chem.*, 2021, **60**, 10280–10290.
26 D. G. Chica, A. K. Iyer, M. Cheng, K. M. Ryan, P. Krantz, C. Laing, R. dos Reis, V. Chandrasekhar, V. P. Dravid and M. G. Kanatzidis, *Inorg. Chem.*, 2021, **60**, 3502–3513.
27 R. Brec*, Solid State Ionics*, 1986, **22**, 3.
28 Y. Kim, N. Arumugam and J. B. Goodenough, *Chem. Mater.*, 2007, **20**, 470–474.
29 P. Bron, S. Johansson, K. Zick, J. S. auf der Günne, S. Dehnen and B. Roling, *J. Am. Chem. Soc.*, 2013, **135**, 15694–15697.
30 M. Ghidiu, J. Ruhl, S. P. Culver and W. G. Zeier, *J. Mater. Chem. A*, 2019, **7**, 17735–17753.
31 W. L. Bragg and G. B. Brown, *Z. Krist.*, 1926, **63**, 538–556.
32 M. Tachez, J. P. Malugani, R. Mercier and G. Robert, *Solid State Ionics*, 1984, **14**, 181–185.
33 P. Fragnaud, E. Prouzet, G. Ouvrard, J. L. Mansot, C. Payen, R. Brec and H. Dexpert, *J. Non. Cryst. Solids*, 1993, **160**, 1–17.
34 R. Pfeiff and R. Kniep, *Z. Naturforsch. B*, 1993, **48**, 1270–1274.
35 Z. Le Huang, J. T. Zhao, J. X. Mi, S. Y. Mao and L. S. Zheng, *J. Solid State Chem.*, 1999, **144**, 388–391.
36 E. G. Gillan and R. B. Kaner, *Chem. Mater.*, 1996, **8**, 333–343.
37 E. -Q. Gao, Z. -M. Wang, and C. -H. Yan, *Chem. Commun.*, 2003, 1748–1749.
38 X. -N. Cheng, W. Xue, J. -H. Huang, and X.-M. Chen, *Dalton Trans.*, 2009, 5701–5707.
39 L. Cheng, W. -X. Zhang, B. -H. Ye, J. -B. Lin, and X. -M. Chen, *Eur. J. Inorg. Chem.* 2007, 2668–2676

